Journal of Engineering Science and Technology
ICIST2023, Vol. 19, No. 2 (2024) 1 - 15

NUMERICAL STUDY OF COOLING AND SOLIDIFICATION IN INJECTION MOULDING: DIRECT FORCING IMMERSED BOUNDARY APPROACH

AVICENNA AN-NIZHAMI[1,*], NANANG APRIANDI[1], IGNATIUS GUNAWAN WIDODO[1], PADANG YANUAR[1], ELFRIDA RIZKY RIADINI[2]

[1]Mechanical Engineering Department, Politeknik Negeri Semarang, Jl. Prof. Sudarto, Tembalang, Kota Semarang, Jawa Tengah, Indonesia, 50275
[2]Mechanical Engineering Department, Universitas Gadjah Mada, Bulaksumur, Yogyakarta, Indonesia, 55281
*Corresponding Author: avicenna@polines.ac.id

Abstract

Injection moulding is a widely used manufacturing method in various industries, necessitating mathematical models to optimise performance, manage costs, and ensure product quality. This study concentrated on elements that have received less attention, notably cooling and solidification in injection moulding. This study investigated how the arrangement of cooling channels affected polymer solidification during the injection moulding. The present study used the Direct Forcing Immersed Boundary (DFIB) method within numerical simulations, employing a finite volume technique. These simulations were carried out in a two-dimensional, time-dependent model encompassing the whole computational domain. The DFIB approach was employed in modelling the solid-liquid interface using a virtual heat term. The in-house numerical code's dependability was confirmed by comparing its findings to analytical results, which revealed a good agreement. The findings suggest that the configuration of cooling channels has a limited impact on the lowest peak temperature, measuring 94.9 °C. However, it notably influences the temperature gradient within a specific region of the polymer surface, with the highest gradient reaching 1178 °C/m. Bringing the cooling channel closer to the polymer surface improved cooling performance. Still, it concurrently resulted in a less uniform temperature distribution, as evidenced by the gradient increasing from 487.1 °C/m to 1178 °C/m. The solidification period of molten polymer varies depending on the configuration of cooling channels and proximity to the surface, with the fastest time at 20.08 seconds for the triple cooling channel.

Keywords: Cooling channel, Direct forcing immersed boundary method, Injection moulding, Solidification, Virtual heat.

1. Introduction

The growth of injection moulding in recent decades has been considerable owing to its wide application in diverse industries such as automotive, electronics, mechanical, and medical. The primary objective of injection moulding is to produce significant quantities and enhance the quality of polymers while keeping the cost minimum. It is crucial to ensure high-quality products and optimise the injection process by carefully controlling the process variables, such as temperature, pressure, and flow rate.

Mathematical models are essential tools for predicting the behaviour of these process variables and optimising the injection process. These models can help manufacturers design better moulds, select suitable materials, and adjust process parameters to achieve optimal performance and reduce costs.

One of the critical advantages of mathematical models is that they can simulate the entire injection moulding process, from filling to cooling, solidification, and ejection. This enables manufacturers to analyse the process in detail and identify potential issues or areas for improvement. For example, by modelling the filling stage, manufacturers can predict the flow behaviour of the plastic material and identify areas of the mould that are likely to experience defects.

By simulating the cooling stage, they can predict the cooling time required to achieve the desired results and optimise the cooling system design. Mathematical models play a critical role in enhancing the injection moulding process and improving the quality of polymer products.

Several investigations have been conducted on the mathematical modelling of the injection moulding process, which encompasses filling, packing, and cooling. One-dimensional models of the filling process in injection moulding have been explored [1-5]. Kamal et al. [6] introduced the development of one-dimensional models for pre- and post-injection processes. The simulation study predicted the progression of the melt front, flow rate, velocity profiles, temperature, and pressure profiles at different times and positions in the cavity and throughout the packing and cooling stages.

Holm and Langtangen [7] used the finite element method to examine the injection moulding process, including cooling, in two dimensions. Chiang et al. [8] developed an integrated fluid and heat transfer model to simulate injection moulding processes to predict shrinkage and warpage. Himasekhar et al. [9] simulated the cooling process of injection moulding using Computer Aided Engineering in three dimensions. Yang et al. [10] investigated the solidification behaviour of high-density polyethylene plastic for various cooling conditions using Enthalpy Transformation Method.

Prasetyo and Fauzun [11] conducted a research study examining the impact of different cooling channel configurations on cooling effectiveness. The findings of their investigation indicate that cooling channels designed in a conformal shape were capable of absorbing significantly more heat compared to channels with a straight configuration.

Hong et al. [12] investigated the characteristics of the solidification process of semi-crystalline thermoplastic polymers during the injection moulding process. The study found that the mechanism of ball formation was examined

experimentally and numerically, revealing that high shear rates during injection moulding and imprinting cause nucleation in micro-cavities.

Kovács and Sikló [13] conducted a numerical study on asymmetric cooling during injection moulding, particularly at mould corners. They found significant temperature differences between mould sides after injecting hot polymer melt. This highlighted the need to address uneven cooling in mould design to prevent part warpage.

Venkatesh et al. [14] conducted a study comparing conformal cooling channels (CCC) and straight-drilled cooling channels (SDCC). Their findings demonstrated that the proposed CCC design improved cycle times and more uniform heat distribution compared to SDCC.

Shen et al. [15] investigated three conformal cooling channels (CCCs) of equal aspect ratio for cooling plastic products. The CCCs significantly reduce the cooling time (10% to 57.1%), ensuring uniform temperature distribution and meeting industrial requirements for fatigue life and stress. He et al. [16] numerically analyse a conformal cooling system for non-pneumatic tire moulds, optimising mould design, reducing cooling time, minimising shrinkage, and ultimately enhancing tire production efficiency and quality.

Solidification is a complex phase transition phenomenon that involves transient heat transfer and a moving interface between solid and fluid phases, which constantly changes due to the heat released by the polymer [17, 18]. This problem is challenging to solve due to the continually moving interface. Cooling processes in injection moulding have been explored in various studies.

However, the cooling dynamics in injection moulding, particularly when coupled with the solidification process, differ significantly due to the unique characteristics of solidification. The solid-liquid interface maintaining a constant temperature during solidification is one of those characteristics. Consequently, the investigation of cooling combined with solidification in the context of injection moulding remains a largely unexplored area in research.

Therefore, this study aims to investigate the impact of cooling channel configuration on the solidification of polymer during injection moulding. In addition, this study utilises an approach for solidification cases using the Direct Forcing Immersed Boundary (DFIB) method. The DFIB method is widely employed for resolving fluid-structure interaction problems, such as flow-induced vibration, wave-induced vibration, and galloping. Nevertheless, this approach remains largely unexplored within the framework of solidification.

2. Numerical Method

The current study utilised in-house numerical software developed using the Fortran programming language. The finite volume technique was implemented to investigate the cooling and solidification process. The software was designed to utilise a computational method known as the DFIB method to simulate such scenarios. The DFIB method's advantageous feature is its ability to utilise a discretised computational domain to simulate multiple scenarios. The forthcoming section, namely Section 2.3, provided a detailed explanation of the DFIB method and its implementation in this investigation.

2.1. Theoretical considerations

Solidification involves multiple phenomena, such as heat transfer and phase change. These phenomena interact with each other and make the problem very complex. Assumptions help to simplify the problem by neglecting certain aspects deemed less necessary or assuming ideal conditions. The study's primary assumptions are as follows:

- The solidification starts when the molten polymer encounters the mould wall, forming a solid/liquid interface [10, 19].
- The initial temperature is T_0, and the contact thermal resistance between the polymer melt and the mould wall is negligible, which means that the polymer surface has the same temperature as the mould wall (T_w) and is much lower than the polymer's phase-change temperature [10, 20].
- The phase change of polymers is assumed to occur at a constant temperature of T_f, which is the reference temperature defined as $T_f = (T_1 + T_2)/2$, where $T_1 - T_2$ represent the phase-change temperature range [10, 21].
- The phase-change process releases latent heat (L_f) at the solid/liquid interface, and the position of the interface varies with time. The interface separates the solid-liquid phase moves until the interfaces meet, indicating the end of the solidification process [10, 19].
- The convection heat transfer in the cooling channel is analysed by applying the DFIB method and solving the governing equation outlined in Sections 2.2 and 2.3. On the other hand, the convection heat transfer occurring at the exterior surface of the mould has been resolved by imposing a boundary condition of convective type.

2.2. Governing equations

The heat from the molten polymer was dissipated through both forced convection to the cooling channels and natural convection to the air surrounding the mould's outer surface. The convection heat transfer coefficient of the cooling channels and its temperature are maintained at a constant value. In order to study this phenomenon, a time-dependent, two-dimensional model was used to simulate the entire computational domain, including the polymer, mould, and cooling channel surfaces. By solving the transient energy equation denoted by Eq. (1), the transient temperature distribution of the mould and polymer can be determined.

$$\rho c_p \frac{\partial T}{\partial t} = k\nabla^2 T \tag{1}$$

where ρ is the density, c_p is the specific heat, T is the temperature, t is time, and k is the thermal conductivity. The heat equation was expressed as a two-dimensional (2D) partial differential equation in a Cartesian coordinate system, denoted by Eq. (2). This formulation specifies the relationship between temperature and its spatial and temporal derivatives in a 2D domain.

$$\rho c_p \frac{\partial T}{\partial t} = k\frac{\partial^2 T}{\partial x^2} + k\frac{\partial^2 T}{\partial y^2} \tag{2}$$

In this study, the second-order partial differential equation was discretised using a second-order central differencing method. The discretisation was performed on a

uniform collocated Cartesian grid. A third-order Adam-Bashforth scheme was utilised for the temporal derivative to ensure third-order accuracy in time integration. The intermediate temperature, T^*, is obtained by solving Eq. (3),

$$T^* = T^n + \Delta t \frac{k}{\rho c_p} \left[\frac{23}{12} B^n - \frac{16}{12} B^{n-1} + \frac{5}{12} B^{n-2}\right] \quad (3)$$

where B , Δt, and superscript n represented the second-order derivative of temperature, time step size and time step level, respectively.

2.3. Direct forcing immersed boundary method

The Direct Forcing Immersed Boundary (DFIB) method is widely utilized in fluid-structure interaction problems, including applications such as the oscillating cylinder in uniform flow [22], cylinder arrays in oscillatory flow [23,24], vortex-induced vibration of circular cylinders [25], and oscillating cylinders beneath a free surface boundary by combining Smoothed Particle Hydrodynamics with DFIB [26]. In this study such method was utilised in this study to model both the cooling channel and moulded part/polymer of injection moulding on a Cartesian grid. In particular, the DFIB method was used to simulate the heat transfer and solidification process. The term "virtual force" in the DFIB method is modified to "virtual heat," which was applied to the heat equation to account for the effects of heat transfer during solidification denoted in Eq. (4).

$$\rho c_p \frac{\partial T}{\partial t} = k \frac{\partial^2 T}{\partial x^2} + k \frac{\partial^2 T}{\partial y^2} + q_v + q_{vc} \quad (4)$$

The virtual heat term of polymer, q_v, and cooling channels, q_{vc}, are the key components in the two distinct types of immersed boundary methods used to model solid-fluid interactions. One such method, developed by Peskin [27], employed smoothed Dirac delta functions to describe this interaction, while the other, proposed by Fadlun et al. [28] and used in the current study, is the direct forcing immersed boundary method. The determination of q_v and q_{vc}, involved calculating the discrepancy between the interpolated temperature and the desired temperature per unit time at each time step at both the cooling channel and the polymer boundaries, which was accomplished using Eqs. (5) and (6), respectively.

$$q_{vc} = \rho c_{pc} \left(\eta_c \frac{T_c - T^*}{\Delta t}\right) \quad (5)$$

$$q_v = \begin{cases} \rho_p c_p \left(\eta_p \frac{T_p - T^*}{\Delta t}\right), & if \;\; T_p = T_f \\ 0, & otherwise \end{cases} \quad (6)$$

In this context, T_c, T^*, T_f, and T_p referred to the cooling channel fluid temperature, intermediate temperature, the melting point temperature of the polymer at which solidification occurred, and polymer temperature, respectively. The cooling channels and polymer were represented as the volume of solid function identified as η_c and η_p, respectively, where η_c and η_p take on values of either 1 or 0. Specifically, η_c equals 1 for the cooling channels and 0 for the moulding and polymer, while η_p equals 1 for the polymer and 0 for the moulding and cooling channels.

$$Q_v = \frac{1}{\Delta t} \int q_v \, dt \quad (7)$$

$$Q_v = \rho_p L_f \frac{\partial f_s}{\partial t} = \rho_p L_f \frac{f_s^{n+1} - f_s^n}{\Delta t} \quad (8)$$

During the solidification process, the virtual heat term, q_v, played a crucial role in ensuring that the temperature of the polymer remains constant. The relationship between the solidification process and the virtual heat term was expressed mathematically in Eqs. (7) and (8), where Q_v was determined by the density of the polymer, ρ_p, the latent heat of the polymer, L_f, and the rate of change of the solid fraction, $\partial f_s/\partial t$. The function $f_s(T_p)$ took on a value of 0 when $T_p > T_f$, and a value of 1 when $T_p < T_f$. In this context, variable Q_v represented the amount of thermal energy that is released from the solid-liquid interface during the process of solidification.

$$T^{n+1} = T^* + [(\Delta t \times q_{vc}^{n+1}) + (\Delta t \times q_v^{n+1})] \quad (9)$$

Upon completion of the solidification calculation, the governing equation was extended by incorporating the virtual heat term, which accounts for the effects of polymer and cooling channels. Subsequently, the final temperature was updated using Eq. (9). The virtual heat terms, namely q_{vc}^{n+1} and q_v^{n+1}, indicated the heat required to maintain the temperature at a constant value or adhere to the pre-determined temperature.

2.4. Computational domain

Each configuration of cooling channels was of identical size, with circular channels having diameters of 30 mm, 15 mm, and 10 mm for the constant perimeter with various position of cooling channels. The separation distance, A, between the cooling channel axis and the polymer substrate had two variabilities by $(0.5D + 5\ \text{mm})$ and $(0.5D + 10\ \text{mm})$, as shown in Fig. 1. The analysis was time-dependent, taking into account.

Changes that occur over time. The operational parameters governing the cooling process and the physical characteristics of the materials involved have been documented in Table 1 and were assumed to remain unchanged throughout all computational outcomes [29]. The spatial domain was discretised in the uniform collocated mesh with the size of 400×400.

Table 1. The values of cooling parameters.

Parameters	Values
Coolant temperature	25 ºC
Injected polymer temperature	180 ºC
Mould initial temperature	60 ºC
Polymer melting temperature	163 ºC
Cooling channel diameter	30, 15, and 10 mm
Latent heat of fusion	115 kJ/kg
Environment temperature	25 ºC
Natural convection coefficient	50 W/m^{2}K
Forced convection coefficient	3650 W/m^{2}K
Mould density	8830 kg/m^3
Mould specific heat	335 J/kg.K
Mould thermal conductivity	250 W/m.K
Polymer density	938 kg/m^3
Polymer specific heat	1800 J/kg.K
Polymer thermal conductivity	0.25 W/m.K

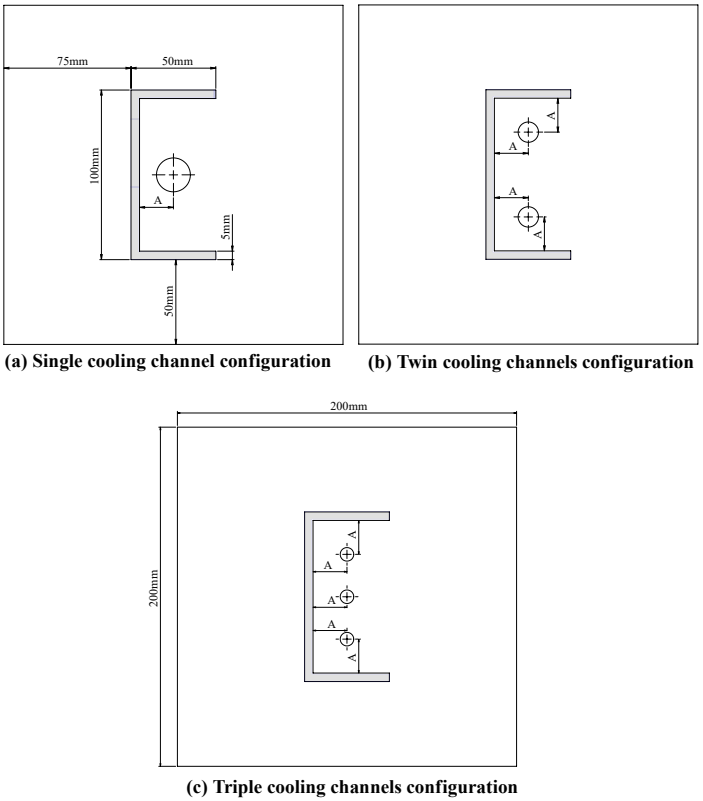

(a) Single cooling channel configuration **(b) Twin cooling channels configuration**

(c) Triple cooling channels configuration

Fig. 1. Geometry and dimensions of computational domains with three various cooling channel configurations.

3. Results and Discussion

This section is divided into two parts: Section 3.1 and Section 3.2. Section 3.1 focuses on validating the in-house numerical code, while Section 3.2 covers the examination of cooling channel configurations, which include the number of cooling channels and the gap between the cooling channels and the polymer surface.

3.1. Validation of in-house numerical code

Validation of numerical methods in solving two-dimensional heat transfer problems, as depicted in Fig. 2, was performed, and a system comprising three sides of a thin rectangular plate was considered. These sides were maintained at a constant temperature of T_{s1}, while the other side was kept at a constant temperature T_{s2}.

The heat transfer from the plate's surface was assumed to be disregarded. The temperature gradient perpendicular to the $x - y$ plane was also assumed to be negligible. Thus, heat transfer occurs exclusively in the x and y directions. The validation results were compared with the analytical method denoted in [30]. The analytical method was derived from the heat diffusion equation, which resulted in Eq. (10). θ represents the normalised temperature difference across the x-y plane, as denoted in Eq. (11).

$$\theta(x,y) = \frac{2}{\pi}\sum_{n=1}^{\infty}\frac{(-1)^{n+1}+1}{n} sin\frac{n\pi x}{L}\frac{sinh(n\pi y/L)}{sinh(n\pi W/L)} \tag{10}$$

$$\theta(x,y) = \frac{T(x,y)-T_{s1}}{T_{s2}-T_{s1}} \tag{11}$$

The temperature distribution was calculated using Eqs. (10) and (11). Additionally, the numerically predicted temperature was extracted along the red dashed line, as depicted in Fig. 2. The utilisation of these analytical and the numerical predictions facilitated a thorough examination of temperature variations and enabling a comprehensive data comparison.

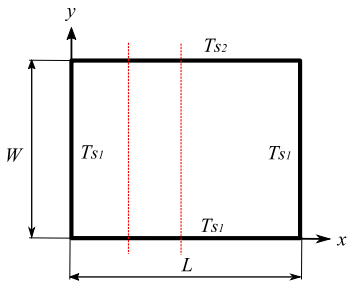

Fig. 2. Validation case (two-dimensional heat transfer).

Figure 3 depicts the validation outcome for θ values along the normalised y coordinate (y/L), where the lines represent the present results, and the symbols represent the analytical results. It is worth noting that due to the symmetrical nature of the case, the validation was conducted at $x/L = 0.25$ and $x/L = 0.5$. The results of the validation demonstrated that the current findings agree well with the analytical result. This agreement indicated that the developed numerical model is reliable in predicting the thermal behaviour of the system. Overall, the validation outcomes demonstrate the effectiveness and accuracy of the developed numerical model in predicting the temperature distribution of the system under consideration.

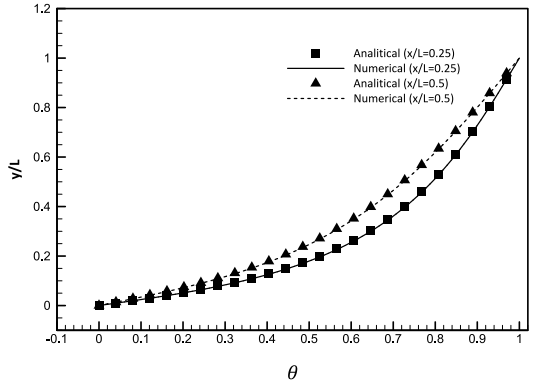

Fig. 3. Temperature distribution along the normalised y coordinate (y/L) at x/L =0.25 and 0.5.

3.2. Parameters study

Figure 4 illustrates the temperature contour in an injection moulding process. it provides valuable insights into the distribution of temperatures within the mould during the cooling phases of the process, which directly impacts the quality of the moulded parts. The contour is represented by a colour gradient, ranging from blue (low temperature) to red (high temperature).

The mould temperature contour is divided into different sections, and each section is colour-coded to depict the temperature distribution. It can be observed that several key features and patterns in the temperature contour. There are distinct areas of higher temperature. These regions represent the molten polymer. Additionally, cooler regions, shown in shades of blue, are visible around the cooling channels or near the mould walls, indicating efficient heat dissipation.

The temperature contour is crucial in injection moulding as it affects various aspects of the process. It influences the quality of the surface finish and the dimensional accuracy of the final moulded parts. Deviations or non-uniformity in the temperature contour can lead to issues like warpage. Warpage refers to the deformation or distortion of a moulded part from its intended shape. Uneven temperature is one of the factors that can contribute to warpage in injection moulding.

The comprehensive examination of the intricate and non-uniform thermal patterns within the solidified polymer plays a pivotal role in ensuring the effective prevention of warping. It is imperative to undertake a thorough analysis, providing a detailed explanation of the uneven dispersion of the temperatures and the accompanying thermal gradients that manifest on the surface of the solidified polymer. This comprehensive investigation allows us to gain a profound understanding of the factor that influence the structural integrity and stability of the solidified polymer. It is worth emphasising that the specific area under analysis pertains to the line segment connecting the points 'a' and 'b' denoted in Fig. 4.

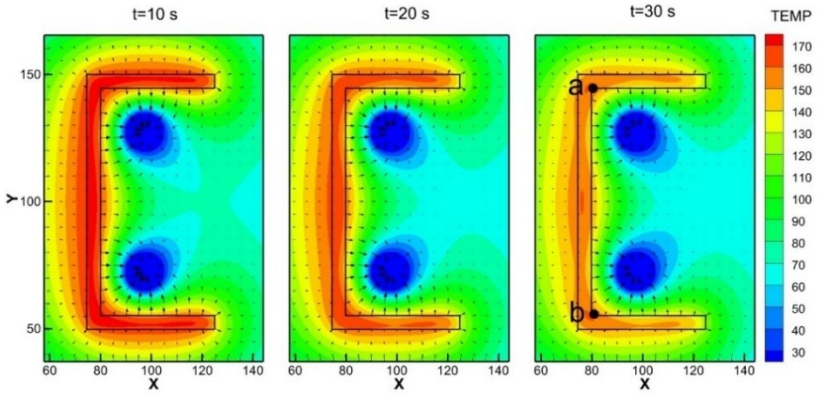

Fig. 4. Evolution of 2D temperature distribution at t=10 s, 20 s, and 30 s.

The investigation delved into analysing temperature distribution and gradient in the y-axis direction. Considering variations of the distance in the axis of the cooling channel and the polymer, denoted as A, across three different cooling channel configurations illustrated in Fig. 5. These figures illustrate the temporal evolution of temperature and its corresponding gradient at specific time intervals, namely 20 s and

40 s. Figure 5 provides insight into the temperature distribution (left) and temperature gradient (right) for the case when A equals (0.5D+10) mm. Interestingly, each configuration exhibits roughly similar lowest temperature values.

The lowest temperature was observed at 40 s with the value 123.5 ºC for the configuration featuring single cooling channels followed by 125.7 ºC and 127.25 ºC for the configuration featuring triple and twin cooling channels, respectively. This suggests that the number of cooling channels with a constant perimeter does not significantly influence the heat flux across the three different cooling channel configurations.

On the other hand, the temperature gradient, dT/dY, which represents the temperature difference across the surface with respect to space in the y-axis direction, has a moderate discrepancy in each configuration. The peak value happens at t=40 s on the triple cooling channel configuration with the value 487.1 ºC/m followed by 473.6 ºC/m, and 332.5 ºC/m for the twin and single cooling channels, respectively.

A notable reduction in temperature accompanied by an amplified temperature gradient is observed when positioning the cooling channel in close proximity to the polymer surface, as illustrated by the dashed line in Fig. 5. The single cooling channel configuration exhibits the lowest temperature, measuring at 94.9 ºC. Conversely, the triple cooling channels configuration demonstrates the highest temperature gradient, reaching 1178 ºC /m. Conversely, for the twin cooling channel at the middle region, when the cooling channel is placed closer, the temperature is higher than the wider distance between the polymer and cooling channel.

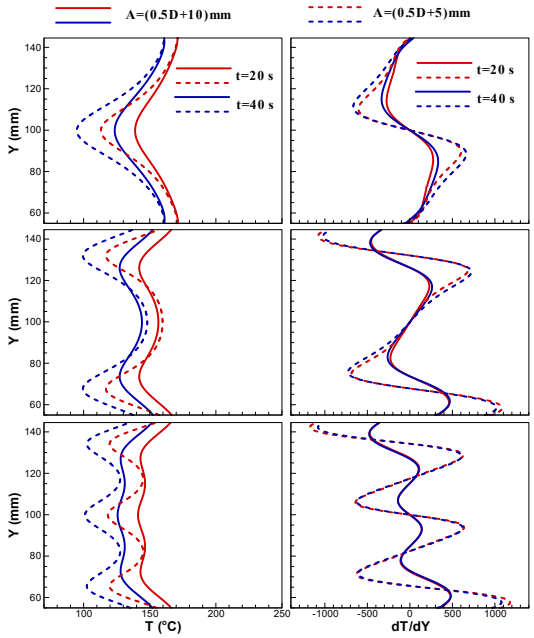

Fig. 5. Evolution of temperature distribution (T) and temperature gradient (dT/dY) in y-axis direction for three cooling channel configurations (from top to bottom: single, twin, and triple cooling channels) at polymer surface (a-b line in Fig. 3).

The investigation required a comprehensive analysis of the temporal progression of solidification across multiple configurations. The investigation was specifically dedicated to examining the divergences in the studied parameters. Figure 6 displays the stages involved in the cooling and solidification of molten polymer. The x-axis represents time in seconds, while the y-axis represents total solidification in percent. It shows a gradual increase in solidification percentage over time as the molten polymer begins to solidify. Initially, the plastic is in a fully molten state, indicated by the lowest solidification point on the graph. As time progresses, the solidification steadily increases, indicating the cooling stage of the injection moulding.

For a single cooling channel, the solidification process initially proceeds slowly and gradually, but after approximately 20 seconds of cooling, it begins to accelerate. Conversely, when the cooling channel is positioned closer to the polymer surface, the solidification percentage experiences an accelerated start, but its rate slows down as the cooling time approaches 20 seconds. The total solidification time for the single cooling channel is 38.05 seconds, with only a negligible improvement observed when the cooling channel is placed closer to the polymer, resulting in a time of 37.03 seconds.

In Fig. 6, the twin cooling channel configuration is depicted by the green line. An unusual occurrence emerges when the cooling channel is positioned in close proximity to the polymer surface. This anomaly manifests at a solidification percentage of approximately 80%. Interestingly, this anomaly does not manifest when the distance between the cooling channel and the polymer is greater. The presence of the anomaly in the twin cooling configuration is attributed to the larger spacing between the cooling channels, which leaves an unsupported region, resulting in lower heat flux. In order to comprehend the peculiar phenomenon, the contours in Fig. 7 are utilised to explain the progression of solidification.

The time history of the solidification percentage, as illustrated in Fig. 6 with the blue line, exhibits the configuration of triple cooling channels. Initially, the solidification line, ranging from 0% to 60%, closely aligns with the twin cooling channel configuration. However, beyond 60% solidification, the lines diverge significantly, creating a noticeable gap. Nonetheless, towards the final stages, the polymer undergoes a slower solidification rate just before complete solidification is achieved.

This deceleration can be attributed to a specific region where the heat flux is extremely low, represented as point P in Fig. 8. Ultimately, the time required to reach complete solidification for both the twin and triple cooling channels is approximately the same, with the twin cooling channel taking 26.8 seconds and the triple cooling channel requiring 26.39 seconds. When the cooling channel placed closer to the polymer surface, the solidification time reach the lowest for the triple cooling channel at 20.08 seconds.

Figures 7 and 8 exhibit the progressive evolution of polymer solidification within an injection mould, featuring an overlay of solidification contours and the heat flux vectors denoted by arrows. The moulded polymer is subdivided into discrete sections. Each assigned a distinct colour to depict the advancement of solidification. The colour spectrum ranges from white, indicating the molten state with zero percentage solidification, to red, signifying complete solidification at 100%.

In the initial stages depicted in the left image of those figures, the red regions in proximity to the cooling channel and corners of the moulded part represent the initial molten polymer introduced into the mould, denoting the beginning of the solidification process. Subsequently, traversing away from the starting point of solidification, a discernible solidification front becomes apparent, particularly in areas exhibiting a higher magnitude of heat flux near the cooling channel. Conversely, regions characterised by the slowest solidification rate are distinguished by minimal heat flux, exemplified by the P points in Figs. 7 and 8.

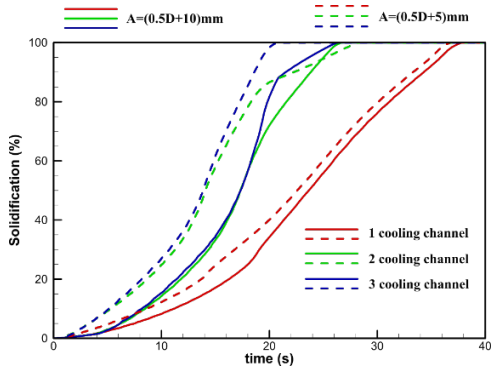

Fig. 6. Time history of total solidification percentage of the polymer during the cooling process.

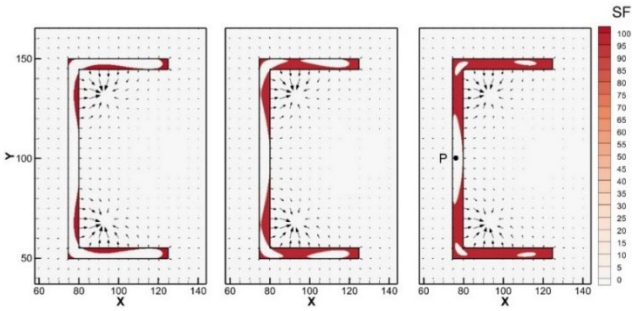

Fig. 7. Evolution of solidification contour with twin cooling channel and $A = (0.5D + 5)$mm at 25%, 50%, and 75% total solidification.

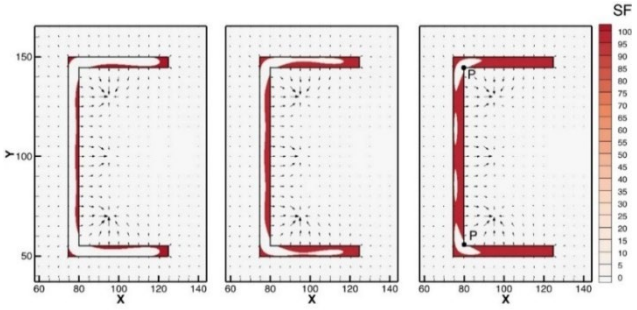

Fig. 8. Evolution of solidification contour with triple cooling channel and $A = (0.5D + 10)$mm at 25%, 50%, and 75% total solidification.

4. Conclusions

The finite volume method was employed for the numerical investigation, and subsequent validation efforts revealed a strong agreement between the numerical and the analytical results. The DFIB method has been utilised to simulate the cooling and solidification process of polymers in injection moulding. Three different cooling channel configurations and two different distances between each cooling channel and the polymer surface were examined.

They were observed by analysing the temperature distribution and its gradient that at a position A = (0.5D+10) mm, the cooling channel configuration had a minimal impact on the lowest peak temperature but had a significant influence on the temperature gradient across the polymer surface. Placing the cooling channel in close proximity at A = (0.5D+5) mm to the polymer surface improved the cooling efficiency, albeit at the expense of achieving uniform temperature distribution across the polymer surface.

The time molten polymer takes to solidify varies depending on the arrangement and distance between the cooling channel and the polymer surface. Increasing the number of cooling channels while keeping the same overall perimeter generally improves the solidification time. Bringing the cooling channels closer to the polymer surface usually helps speed up solidification, except in the case of twin cooling channels where it makes the solidification time longer.

Nomenclatures

A	Cooling channel axis and polymer distance.
B	Second-order derivative of temperature.
c_p	Specific heat of polymer, J/kg.K.
c_{pc}	Specific heat of cooling channel, J/kg.K.
D	Diameter of the cooling channel
f_s	Solid fraction.
k	Thermal conductivity.
L_f	Latent heat of the polymer, kJ/kg.
n	Time step level.
q_v	Virtual heat of polymer, J/m^3.
q_{cv}	Virtual heat of cooling channel, J/m^3.
t	Time, s.
T^*	Intermediate temperature, ^{0}C.
T_0	Initial temperature, ^{0}C.
$T_1 - T_2$	Phase-change temperature range, ^{0}C.
T_p	Phase-change temperature range, ^{0}C.
T_s	Surface temperature of validation case, ^{0}C.
T_f	Melting point temperature of the polymer, ^{0}C.
T_w	Mould wall temperature, ^{0}C.

Greek Symbols

Δt	Time step size, s.
ρ	The density of material, kg/ m^3.
η_c	The volume of the cooling channel function.
η_p	The volume of polymer function.
θ	Non-dimensional temperature difference.

Abbreviations

DFIB	Direct forcing immersed boundary

References

1. Wu, P.C.; Huang, C.F.; and Gogos, C.G. (1974). Simulation of the mold-filling process. *Polymer Engineering and Science*, 14(3), 223-230.
2. Stevenson, J.F. (1978). A simplified method for analysing mold filling dynamics part I: Theory. *Polymer Engineering and Science*, 18(7), 577-582.
3. Stevenson, J.F.; and Chuck, W. (1979). A simplified method for analysing mold filling dynamics. Part II: Extensions and comparisons with experiment. *Polymer Engineering and Science*, 19(12), 849-857.
4. Harry, D.H.; and Parrott, R.G. (1970). Numerical simulation of injection mold filling. *Polymer Engineering and Science*, 10(4), 209-214.
5. Williams, G.; and Lord, H.A. (1975). Mold-filling studies for the injection molding of thermoplastic materials. Part I: The flow of plastic materials in hot- and cold-walled circular channels. *Polymer Engineering and Science*, 15(8), 553-568.
6. Kamal, M.R.; and Kenigo, S. (1972). The injection molding of thermoplastics part I: Theoretical model. *Polymer Engineering and Science*, 12(4), 294-301.
7. Holm, E.J.; and Langtangen, H.P. (1999). A unified finite element model for the injection molding process. *Computer Method in Applied Mechanics and Engineering*, 178(3-4), 413-429.
8. Chiang, H.H.; Himasekhar, K.; Santhanam, N.; and Wang, K.K. (1993). Integrated simulation of fluid flow and heat transfer in injection molding for the prediction of shrinkage and warpage. *Journal of Engineering Materials and Technology*, 115(1), 37-47.
9. Himasekhar, K.; Lottey, J.; and Wang, K.K. (1992). CAE of mold cooling in injection molding using a three-dimensional numerical simulation. *Journal of Engineering for Industry*, 144(2), 213-221.
10. Yang, B.; Miao, J.B.; Min, K.; Xia, R.; Qian, J.S.; and Wang, X. (2013). Solidification behavior of high-density polyethylene during injection molding process: Enthalpy transformation method. *Journal of Applied Polymer Science*, 128(3), 1922-1929.
11. Prasetiyo, A.B.; and Fauzun, F. (2018). Numerical study of effect of cooling channel configuration and size on the product cooling effectiveness in the plastic injection molding. *Proceeding of the 3rd Annual Applied Science and Engineering Conference* (*AASEC 2018*), 197.
12. Hong, J.; Kim, S.K.; and Cho, Y.H. (2020). Flow and solidification of semi-crystalline polymer during micro-injection molding. *International Journal of Heat and Mass Transfer*, 153.
13. Kovács, J.G.; and Sikló, B. (2011). Investigation of cooling effect at corners in injection molding. *International Communications in Heat and Mass Transfer*, 38(10), 1330-1334.
14. Venkatesh, G.; Kumar, Y.R.; and Raghavendra, G. (2017). Comparison of straight line to conformal cooling channel in injection molding. *Materials Today: Proceedings*, 4(2), 1167-1173.
15. Shen, S.; Kanbur, B.B.; Zhou, Y.; and Duan, F. (2020). Thermal and mechanical analysis for conformal cooling channel in plastic injection molding. *Materials Today: Proceedings*, 28(2), 396-401.

16. He, H.; Xing, Y.; Wang, R.G.; Lu, Y.L.; Zhang, L.Q. and Li, F.Z. (2023). Optimisation design of cooling system for injection molding mold of non-pneumatic tire. *Thermal Science and Engineering Progress*, 42.
17. Carslaw H.S; and Jaeger J.C. (1959). *Conduction of heat in solids*. Clarendon Press, Oxford.
18. Goodman, T.R.; and Shea, J.J. (1960). The melting of finite slabs. *Journal of Applied Mechanics*, 27(1), 16-24.
19. Yang, B.; Fu, X.R.; Yang, W.; Sun, N.; Hu, S.; Lu, Y.; and Yang, M.B. (2010). Prediction of heat conduction with phase-change effects during cooling stage of injection molding of high-density polyethylene: approximate integral approach. *Journal of Macromolecular Science, Part B*, 49(4), 734-749.
20. Yang, B.; Fu, X.R.; Yang, W.; Liang, S.P.; Sun, N.; Hu, S.; and Yang, M.B. (2009). Effect of melt and mold temperatures on the solidification behavior of HDPE during gas-assisted injection molding: An enthalpy transformation approach. *Macromolecular Materials and Engineering*, 294(5), 336-344.
21. Cho, S.H.; and Sunderland, J.E. (1969). Heat-conduction problems with melting or freezing. *ASME Journal of Heat and Mass Transfer*, 91(3),421-426.
22. Noor, D.Z.; Chern, M.J.; and Horng, T.L. (2009). An immersed boundary method to solve fluid-solid interaction problems. *Computational Mechanics*, 44(4), 447-453.
23. Chern, M.J.; Hsu, W.C.; and Horng, T.L. (2012). Numerical prediction of hydrodynamic loading on circular cylinder array in oscillatory flow using direct-forcing immersed boundary method. *Journal of Applied Mathematics*, 2012, 1-16.
24. Chern, M.J.; Shiu, W.C.; and Horng, T.L. (2013). Immersed boundary modeling for interaction of oscillatory flow with cylinder array under effects of flow direction and cylinder arrangement. *Journal of Fluids and Structures*, 43, 325-346.
25. Chern, M.J.; Kuan, Y.H.; Nugroho, G.; Lu, G.T.; and Horng, T.L. (2014). Direct-forcing immersed boundary modeling of vortex-induced vibration of a circular cylinder. *Journal of Wind Engineering and Industrial Aerodynamics*, 134, 109-121.
26. Moballa, B.; Chern, M.-J.; An-Nizhami, A.; and Borthwick, A.G.L. (2019). DFIB-SPH study of submerged horizontal cylinder oscillated close to the free surface of a viscous liquid. *Fluid Dynamics Research*, 51(3), 035506.
27. Peskin, C.S. (1972). Flow patterns around heart valves: A numerical method. *Journal of Computational Physics*, 10(2), 252-271.
28. Fadlun, E.A.; Verzicco, R.; Orlandi, P.; and Mohd-Yusof, J. (2000). Combined immersed-boundary finite-difference methods for three-dimensional complex flow simulations. *Journal of Computational Physics*, 161(1), 35-60.
29. Qiao, H. (2005). Transient mold cooling analysis using BEM with the time-dependent fundamental solution. *International Communications in Heat and Mass Transfer*, 32(3-4), 315-322.
30. Faghri, A.; Zhang, Y.W.; and Howell, J.R. (2010). *Advanced heat and mass transfer*. Global Digital Press.